Journal of Electrochemistry

Volume 25 | Issue 6

2019-12-28

An Aptasensor Based on AuNPs/PANI/TNTs Nanocomposite for Electrochemical Detection of Tobramycin

Yong-ling NONG

Ni-na QIAO

Ying LIANG
School of Chemistry and Chemical Engineering, GuangDong Pharmaceutical University, Guangzhou, 510006, China;Guangdong Cosmetics Engineering & Technology Research Center, Guangzhou, 510006, China;, lyingair@126.com

Recommended Citation
Yong-ling NONG, Ni-na QIAO, Ying LIANG. An Aptasensor Based on AuNPs/PANI/TNTs Nanocomposite for Electrochemical Detection of Tobramycin[J]. *Journal of Electrochemistry*, 2019 , 25(6): 720-730.
DOI: 10.13208/j.electrochem.180612
Available at: https://jelectrochem.xmu.edu.cn/journal/vol25/iss6/9

This Article is brought to you for free and open access by Journal of Electrochemistry. It has been accepted for inclusion in Journal of Electrochemistry by an authorized editor of Journal of Electrochemistry.

DOI: 10.13208/j.electrochem.180612 **Artical ID**:1006-3471(2019)06-0720-11
Cite this: *J. Electrochem.* **2019**, *25*(6): 720-730 **Http**://electrochem.xmu.edu.cn

An Aptasensor Based on AuNPs/PANI/TNTs Nanocomposite for Electrochemical Detection of Tobramycin

NONG Yong-ling[1], QIAO Ni-na[1], LIANG Ying[1,2*]

(1. *School of Chemistry and Chemical Engineering, GuangDong Pharmaceutical University, Guangzhou,* 510006, *China*; 2. *Guangdong Cosmetics Engineering & Technology Research Center, Guangzhou*, 510006, *China*)

Abstract: A novel well-constructed electrochemical aptamer-based sensor for the detection of tobramycin was presented, using differential pulse voltammetry (DPV) as a detection technique and methylene blue (MB) as an electrochemical indicator. A glassy carbon electrode modified with a nanocomposite of Au nanoparticles/polyaniline/titania nanotubes (AuNPs/PANI/TNTs) was constructed as the electrode scaffold. The nanocomposite was characterized by transmission electron microscopy and X-ray photoelectron spectroscopy in detail. The results of cyclic voltammetry and electrochemical impedance measurements demonstrated that the AuNPs/PANI/TNTs nanocomposites can improve greatly the electron transfer on the interface. For the detection of tobramycin, the DPV results showed a linear relationship between the current response and the concentration of tobramycin, and a wide range of detection from 0.5 $\mu mol \cdot L^{-1}$ to 70 $\mu mol \cdot L^{-1}$. The presented aptamer-based biosensor exhibited excellent sensitivity and reproducibility, which would have a potential application in bioanalysis and clinical diagnostics.

Key words: aptasensor; tobramycin; electrochemical analysis; Au nanoparticles

CLC Number: O646 **Document Code:** A

Tobramycin, as an aminoglycoside antibiotic, provides bactericidal activity against various types of bacterial infections, particularly Pseudomonas[1]. During the process of disease treatment, tobramycin has exhibited bad side effects, such as ototoxicity and nephrotoxicity. Suitable dosing of the drug is critical to obtain high drug efficiency and low side effects. Therefore, it is vital to monitor the serum levels of tobramycin during therapy. However, the detection of tobramycin with high sensitivity is difficult due to its poor chromophore effects and poor stability. In addition, the narrow therapeutic range (4.3 ~ 25.7 $\mu mol \cdot L^{-1}$) in serum make tobramycin more complicated to be monitored[2]. Therefore, the development of reliable and high sensitive methods for the detection of tobramycin is challenging.

Several methods, such as microbiological assays, immunoassays, high performance liquid chromatography (HPLC), and capillary electrophoresis (CE), have been developed for the analysis of tobramycin in complex biological matrices[3-4]. However, these methods have limitations more or less. For example, microbiological assays are time consuming, non-specific, and show poor sensitivity[5]. Among the various methods developed thus far, electrochemical biosensors have attracted tremendous focuses and efforts because of their simplicity, high sensitivity and stability, and on-site analysis[6-9]. Aptamer-based electrochemical biosensors have been studied for the detection of tobramycin[10-13]. Zhang and co-workers fabricated SnO_x@TiO_2@mC nanocomposites as the scaffold materials for the electrochemical aptasensor. They confirmed the tobramycin detection by EIS method, and showed high sensitivity and a broad detection range of tobramycin[14].

Aptamer with single-stranded DNA or RNA oligonucleotides has been extensively selected for binding to specific target molecules due to its unique structure, such as a hairpin structure. For the aptamer-based biosensors, probe packing density on the

Received: 2018-06-12, Revised: 2018-08-10 *Corresponding author, Tel: (86-20)88207262, E-mail: lyingair@126.com

electrode surface and the redox tag employed has great impact on the sensitivity and the observed affinity. Here an aptamer of 27-mer RNA sequence [15-16] was used as the recognition element. Methylene blue (MB) was chosen as a redox tag because it intercalates with RNA[17-19] and possesses good redox properties. Tobramycin is easily encapsulated within the aptamer loop and capped by the looped-out base, so the aptamer prefers to bind with tobramycin molecules rather than with MB. When tobramycin is introduced, the strong interaction between tobramycin and the aptamer makes MB being released from the aptamer surface, resulting in a reduced signal from the adsorbed MB.

The electrode materials as a scaffold have great influence on the efficiency of electrochemical biosensors. Generally speaking, possessing higher bioaffinity and better electronic conductivities would provide higher electrochemical activity. AuNPs with unique properties of large specific surface area, essential nontoxicity, excellent biocompatibility, and good conductivity, are often chosen as electrode materials[12-13, 20-22]. Moreover, AuNPs could tightly bind to the modified SH aptamer based on gold-thiol chemistry and the functionalized AuNPs with aptamers have also been used for the amplified optical detection of proteins in the sandwich configuration[23]. TiO_2 nanotubes (TNTs) can be used as an excellent support for the loading of metal nanoparticles to enhance the catalytic efficiency[24]. Polyaniline (PANI) is a conductive polymer with an acid/base doping response, which makes it attractive in the field of biosensor. In this study, the composites of AuNPs deposited on TNTs decorated with PANI (AuNPs/PANI/TNTs) were prepared as the immobilization interface.

Combining the benefits of good biocompatibility of AuNPs and TiO_2 nanotubes wiht the excellent conductivity of PANI, we successfully prepared an aptamer-based sensor, supported with a AuNPs/PANI/TNTs nanocomposite, using MB as the electrochemical signal for the detection of tobramycin. The architecture of the composite allowed for efficient electron transfer via the immobilized aptamer and high sensitivity. The results indicated that the amperometric response has a good linear relation with the concentration of tobramycin.

1 Experimental

1.1 Chemicals

The oligonucleotide RNA aptamer, with a 5'-SH modification, was purchased from Sangon Biotech Co., Ltd. (Shanghai, China); the base sequence of the aptamer was as follows: 5'-SH-(GGCACGAGGUUUAGCUACACUCGUGCC-3')[11].

The TiO_2 nanoparticles (P25) were purchased from Tianjin Chemical Reagent Co., Ltd. China. Tobramycin, bovine serum albumin (BSA), ammonium persulfate (APS, 98%), aniline hydrochloride, gold (III) chloride trihydrate ($HAuCl_4 \cdot 3H_2O$), trisodium citrate, sodium borohydride ($NaBH_4$), MB, $K_3Fe(CN)_6$, $K_4Fe(CN)_6 \cdot 3H_2O$ and all other reagents (obtained from Sinopharm or Aladdin) were used without further purification. The ultrapure water (18 MΩ·cm) prepared by purification was used. Phosphate buffer solutions (PBS) were prepared with NaH_2PO_4 and Na_2HPO_4.

1.2 Preparation of the AuNPs/PANI/TNTs Composites

TNTs were fabricated using an established hydrothermal reaction method[25-26]. Briefly, a mixture of 0.6 g P25 and 120 mL of 10 mol·L^{-1} NaOH was reacted in a Teflon-lined autoclave at a temperature of 120 ℃ for 48 h. The obtained white coarse products were treated with a solution of 0.1 mol·L^{-1} aqueous HCl and distilled water, then the sample was washed, centrifuged, dried and stored in vacuum oven for use.

The synthesis of the composites of PANI/TNTs was as follows: a solution of 8.57 mL aniline hydrochloride (0.1 mol·L^{-1}) and 10 mL of HCl (0.1 mol·L^{-1}) was prepared; then, 0.2660 g TNTs was dispersed into the above mixture under magnetic stirring for 30 min in an ice water bath. Subsequently, 8.57 mL APS solution (0.1 mol·L^{-1}) was added drop-wise to the suspension and stirred for over 5 h at 0 ~ 5 ℃. The obtained sample was washed with water several times, and dried and ground to get a fine powder.

18 mg PANI/TNTs was dispersed in 18 mL water. 1 mL $HAuCl_4$ (0.01 mol·L^{-1}) and 1 mL of 0.01 mol·L^{-1}

sodium citrate were added into the uniform suspension with continuous stirring. Afterward, 1 mL $NaBH_4$ solution (0.1 mol·L^{-1}, 0 ℃ ~ 4 ℃) was added to the suspension with stirring vigorously. The obtained product was washed and dried, and designated as AuNPs/PANI/TNTs composite.

1.3 Fabrication of the Aptasensor

The electrochemical electrode was prepared as follows: briefly, 5 mg of the AuNPs/PANI/TNTs composite was dispersed in 1 mL of 0.2% chitosan solution and ultrasonicated to obtain a uniform mixture. Then, 5 μL of this mixture was deposited on the previously polished surface of glassy carbon (GC) electrode and dried at an ambient temperature. The prepared electrode was designated as AuNPs/PANI/TNTs/GC.

Subsequently, 20 μL of 130 μmol·L^{-1} aptamer was deposited on the surface of the AuNPs/PANI/TNTs/GC electrode and incubated for 12 h at ambient temperature. After the aptamer layer had been formed, the prepared electrode (designated as Apt/AuNPs/PANI/TNTs/GC) was rinsed carefully with 0.1 mol·L^{-1} PBS solution (pH 7.0) to remove the excess and non-specifically adsorbed RNA. Then, 10 μL 1% BSA solution was deposited on the surface of the electrode and retained for 30 min to reduce non-specific binding. Subsequently, the electrode was immersed in 20 μmol·L^{-1} MB of PBS solution for 15 min. The fabricated electrode (designated as MB/Apt/AuNPs/PANI/TNTs/GC) was washed by rinsing with water and PBS successively several times. At last, the electrode was immersed into solutions of tobramycin for 40 min for electrochemical analysis.

1.4 Characterizations of Nanomaterials

The morphologies of the nanomaterials were examined by transmissi on electron microscope (TEM, Hitachi, H-7650). X-ray photoelectron spectroscopic (XPS) analysis was conducted using an ESCALAB 250 (Thermo Scientific, USA). Cyclic voltammetry (CV), differential pulse voltammetry (DPV), and electrochemical impedance spectroscopic (EIS) measurements were performed using a CHI660E Electrochemical Workstation (Shanghai CHI Instrument Co., China) in conjunction with a conventional three-electrode system. A GC electrode modified with different samples acted as the working electrode, the platinum sheet electrode as the auxiliary electrode, and Ag/AgCl electrode as the reference electrode. EIS was conducted in 0.1 mol·L^{-1} KCl solution containing 5 mmol·L^{-1} $K_3[Fe(CN)_6]/K_4[Fe(CN)_6]$ (1:1) at a modulation voltage of 5 mV with the frequency ranging from 0.1 Hz to 100 kHz. The faradaic impedance spectra were fitted using the Zview modeling program (Version 3.1). All electrochemical measurements were carried out in a nitrogen-saturated enviroment at room temperature. The electrochemical signals of DPV were measured in PBS with an amplitude of 25 mV.

2 Results and Discussion

2.1 Principle of the Tobramycin Detection

The detection principle of the electrochemical aptasensor for tobramycin is illustrated in Scheme 1. Initially, the surface of the GC electrode was modified with a homogeneous film of AuNPs/PANI/TNTs nanocomposite, which would increase the electrochemical active area. The 5'-SH-modified aptamer was site-specifically attached to the AuNPs by the gold-thiol chemical bonds. Then, MB was intercalated into the aptamer interacted with G-C bond or guanine bases[18], which produced a clear DPV signal denoted as “a” in Scheme 1. But the DPV signal of MB decreased (denoted as “b” in Scheme 1), when tobramycin was introduced. Tobramycin bound to the RNA major groove centered about a stem-loop junction site[16]. Because the interaction of aptamer with tobramycin overwhelmed that of MB, so some of MB discharged off from the surface of the aptamer. The similar formation of the aptamer-target complex on the modified electrode surface could also be found by Zhang et al. [27] and Khezrian et al[28].

2.2 Characterizations of the Electrode Materials

The morphologies of the TNTs and AuNPs/PANI/TNTs nanocomposite were characterized by TEM (Fig. 1). The TEM image of TNTs showed tubular morphology, with a mean diameter of approximately

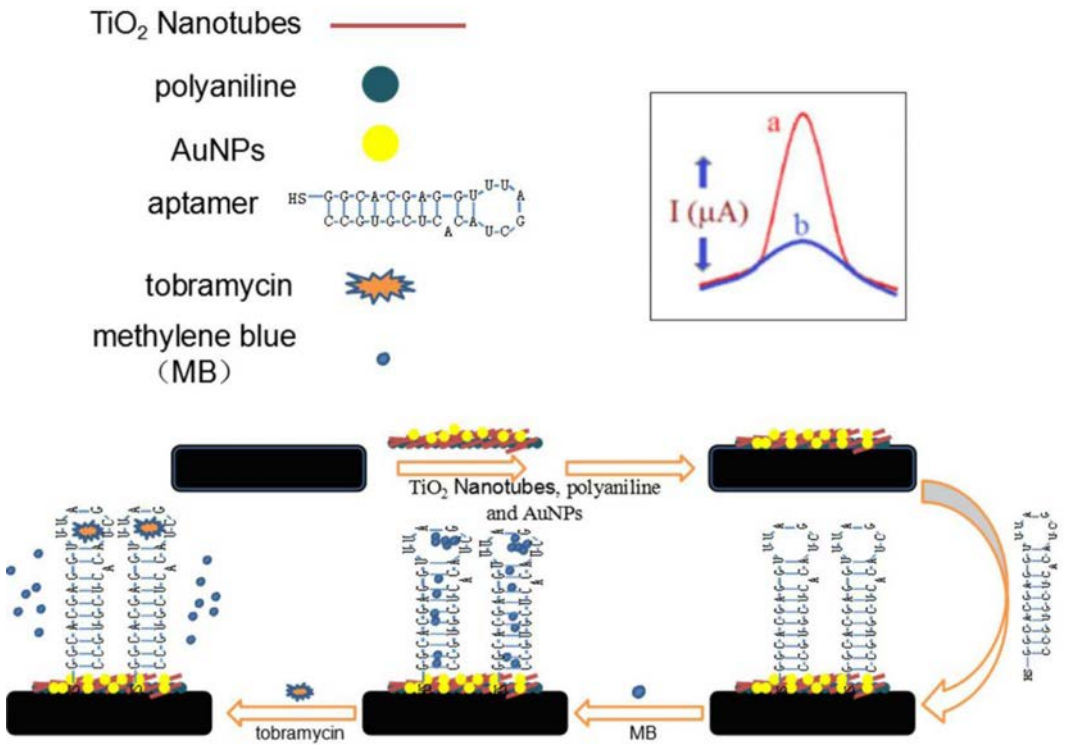

Scheme.1 Schematic diagram of the principle for the aptasensor

10 nm (Fig. 1A), indicating that TNTs were successfully synthesized[29-30]. From Fig. 1B, it can be seen that AuNPs dispersed uniformly on the surface of the PANI/TNTs composite. The AuNPs have an average size of 4 nm by counting 100 particles.

XPS measurements were carried out to disclose the electronic state of different elements. The signals of Ti2p, O1s, C1s, N1s, Au4d, and Au4f were detected, which arose from AuNPs/PANI/TNTs composite (Fig. 2A)[31-32]. The peaks at 458.8 and 464.5 eV were assigned to $Ti2p_{3/2}$ and $Ti2p_{1/2}$, respectively (Fig. 2B)[33-34]. The O1s spectrum located at 530.5 and 532.2 eV (Fig. 2C) was attributed to the Ti-OH groups and the lattice oxygen [Ti-O_6], respectively[34-35]. The N1s spectrum exhibited a peak at 399.2 eV, which was ascribed to the benzenoid amine (-NH-) in PANI. The XPS spectrum of Au4f was separated to two peaks centered at 83.68 eV and 87.47 eV (Fig. 2E), assigned to the metallic state of Au[32], suggesting that Au^{3+} was reduced successfully to form AuNPs.

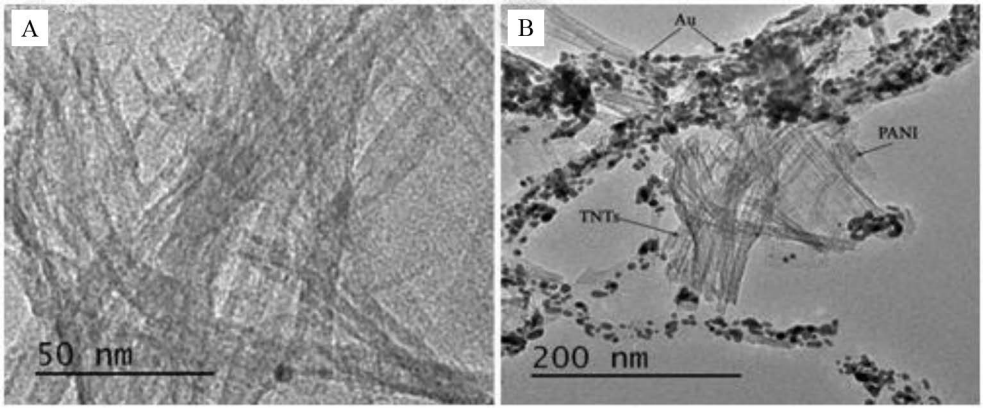

Fig. 1 TEM images of (A) TNTs and (B) AuNPs/PANI/TNTs

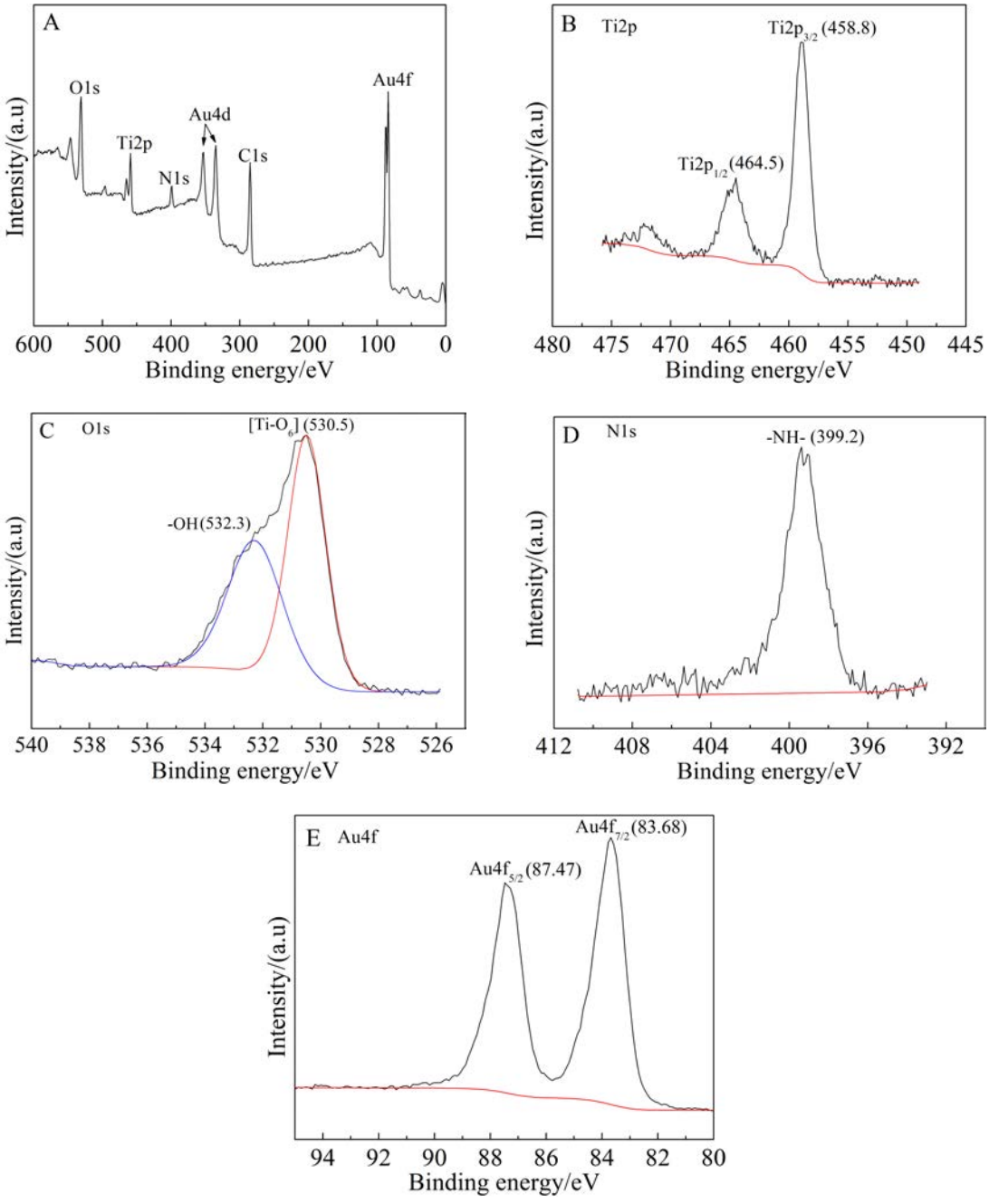

Fig. 2 XPS survey spectra (A), and high-resolution XPS spectra of (B) Ti2p, (C) O1s, (D) N1s and (E) Au4f of AuNPs/PANI/TNTs composite

Fig. 3 represents electrochemical characterization of electrode materials. To investigate the interaction of tobramycin and aptamer, the Apt/AuNPs/PANI/TNTs/GC electrode, immersed in 5 μmol·L^{-1} tobramycin (denoted as 5 μmol·L^{-1} TBR/Apt/AuNPs/PANI/TNTs/GC), was also prepared for comparison. Fig. 3A shows the CVs of 5.0 mmol·L^{-1} $[Fe(CN)_6]^{3-/4-}$ in 0.1 mol·L^{-1} KCl solution. A pair of redox peaks for $[Fe(CN)_6]^{3-/4-}$ on all the electrodes occurred (Fig. 3A). On the GC electrode, a ΔEp of 0.179 V was obtained. After implementing the modification of AuNPs/PANI/TNTs nanocomposite, the current response increased significantly and ΔEp decreased to 0.137 V; this demonstrated that the incorporation of this nanocomposite provided a greater electron transfer compared with that of GC electrodes. After the aptamer was

modified on the AuNPs/PANI/TNTs/GC, the peak current of $[Fe(CN)_6]^{3-/4-}$ decreased. It is possible that the electrode surface bound with the aptamer would block the efficiency of electron transfer because of the aptamer's repulsion with the anionic $[Fe(CN)_6]^{3-/4-}$. Expectedly, the peak current decreased largely with the incubation with 5 μmol·L^{-1} tobramycin for 40 min (Fig. 3A), which implied that tobramycin had been immobilized to the electrode successfully.

The interface properties of different electrodes were investigated by electrochemical impedance spectroscopy (EIS). Fig. 3B demonstrates the impedance spectra obtained using the GC, AuNPs/PANI/TNTs/GC, Apt/AuNPs/PANI/TNTs/GC, and the 5 μmol·L^{-1} TBR/Apt/AuNPs/PANI/TNTs/GC electroctrodes in 0.1 mol·L^{-1} KCl solution containing 5 mmol·L^{-1} $[Fe(CN)_6]^{3-/4-}$. A semicircle portion at higher frequencies and a linear part at lower frequencies were observed, which corresponded to the electron transfer-limited process and diffusion process, respectively. A modified Randle's equivalent circuit was used to fit the EIS data and the results are shown in the inset (C) of Fig. 3B. Here, R_s represents the electrolyte resistance, CPE is the constant phase elecment, R_{ct} is the charge-transfer resistance, and Z_w is the Warburg impedance. Generally, the value of R_{ct} can be used to characterize the electrode properties. The values of R_{ct} for different electrodes achieved by fitting the experimental data are shown in Tab. 1. The

Tab. 1 Values of equivalent circuit elements R_{ct} for different electrodes, the numbers in parentheses refer to the RSD for each value (n = 3).

Electrode	R_{ct}/Ω
GC	135.4 (1.2)
AuNPs/PANI/TNT/GC	23.6 (5.9)
Apt/AuNPs/PANI/TNT/GC	158.6 (1.5)
5 μmol·L^{-1} TBR/Apt/AuNPs/PANI/TNT/GC	395.6 (0.5)

R_{ct} value of the AuNPs/PANI/TNTs/GC electrode decreased considerably from 135.4 Ω to 23.6 Ω as compared with that of the bare GC electrode. This indicated that the modified electrode had a higher electron transfer ability, which might be attributed to the larger electrochemical surface area and good electrical conductivity after modifying with the nanocomposite. When the aptamer was immobilized on AuNPs/PANI/TNTs/GC, the R_{ct} value increased to 158.6 Ω, indicating that Apt blocked the transfer of electrons.

The 5 μmol·L^{-1} TBR/Apt/AuNPs/PANI/TNTs/GC electrode exhibited an increase in R_{ct} up to 395.6 Ω, suggesting that the strong interaction of TBR and Apt was achieved. The results of EIS were consistent with those of the CVs (Fig. 3A), which also demonstrated that the sensing interface was successfully constructed.

CVs of the MB/Apt/AuNPs/PANI/TNTs/GC

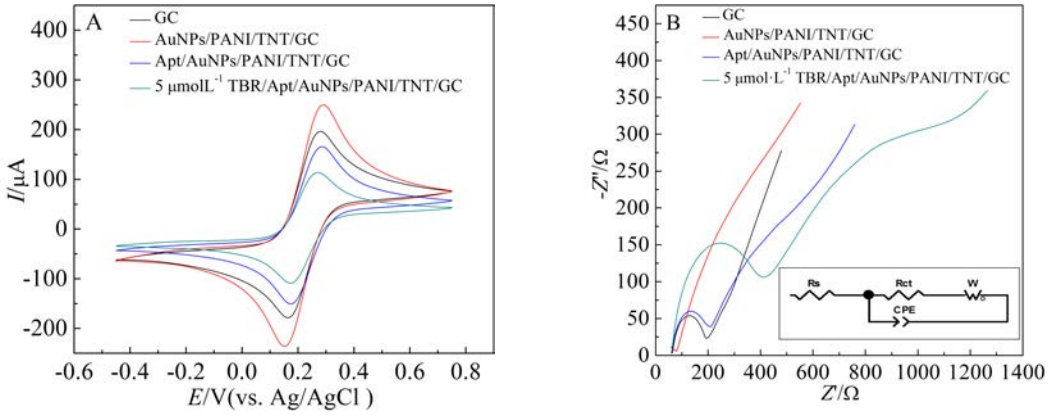

Fig. 3 (A) CVs and (B) Nyquist plots of 5.0 mmol·L^{-1} $[Fe(CN)_6]^{3-/4-}$ in 0.1 mol·L^{-1} KCl on bare GC, AuNPs/PANI/TNTs/GC, Apt/AuNPs/PANI/TNTs/GC and 5 μmol·L^{-1} TBR/Apt/AuNPs PANI/TNTs/GC electrodes (scan rate: 0.1 V·s^{-1}; frequency range: 0.1 ~ 10 kHz)

electrode at different scan rates are shown in Fig. S1 (supplementary materials). As expected, the peak currents of the redox system were proportional to the scan rates in the range of 10 to 100 mV·s^{-1} (the inset (A) in Fig. S1), indicating that surface-controlled electrochemical process was a rate determining step. The factors that affected the condition of the sensor, such as concentration of the aptamer, pH value of the solution, and reaction time, were investigated in detail (Fig. S2). The results show that 130 μmol·L^{-1} was the optimal concentration of the aptamer, pH 7.0 was the best, and 40 min was the optimal incubation time. Additionally, the reusability of the electrode system was examined and the result is shown in Fig S3. There was a 3.2% decrease of peak current for the 100th repetitive time, indicating that the redox system of MB and voltammetric behavior of the nanomaterials were stable.

2.3 Characterizations of the Aptasensor

A quantitative analysis of sensitive target molecules at different concentrations of tobramycin was conducted. Fig. 4 shows the electrochemical responses of the MB/Apt/AuNPs/PANI/TNTs/GC electrode after incubation with different concentrations of tobramycin for 40 min. The lower concentration range from 0.5 to 4.0 μmol·L^{-1} and the higher concentration range from 5 to 70 μmol·L^{-1} are shown in Fig. 4A and Fig. 4B, respectively. As the concentration of tobramycin increased, the signals of the MB peak current decreased. The decrease in DPV signal of MB may be attributed to two reasons. Because the interaction of aptamer with tobramycin overwhelmed that of MB, so some of MB discharged off from the surface of the aptamer after the modified electrode incubated with tobramycin. On the other hand, from Fig. 3 and Tab. 1, it can be inferred that the strong in-

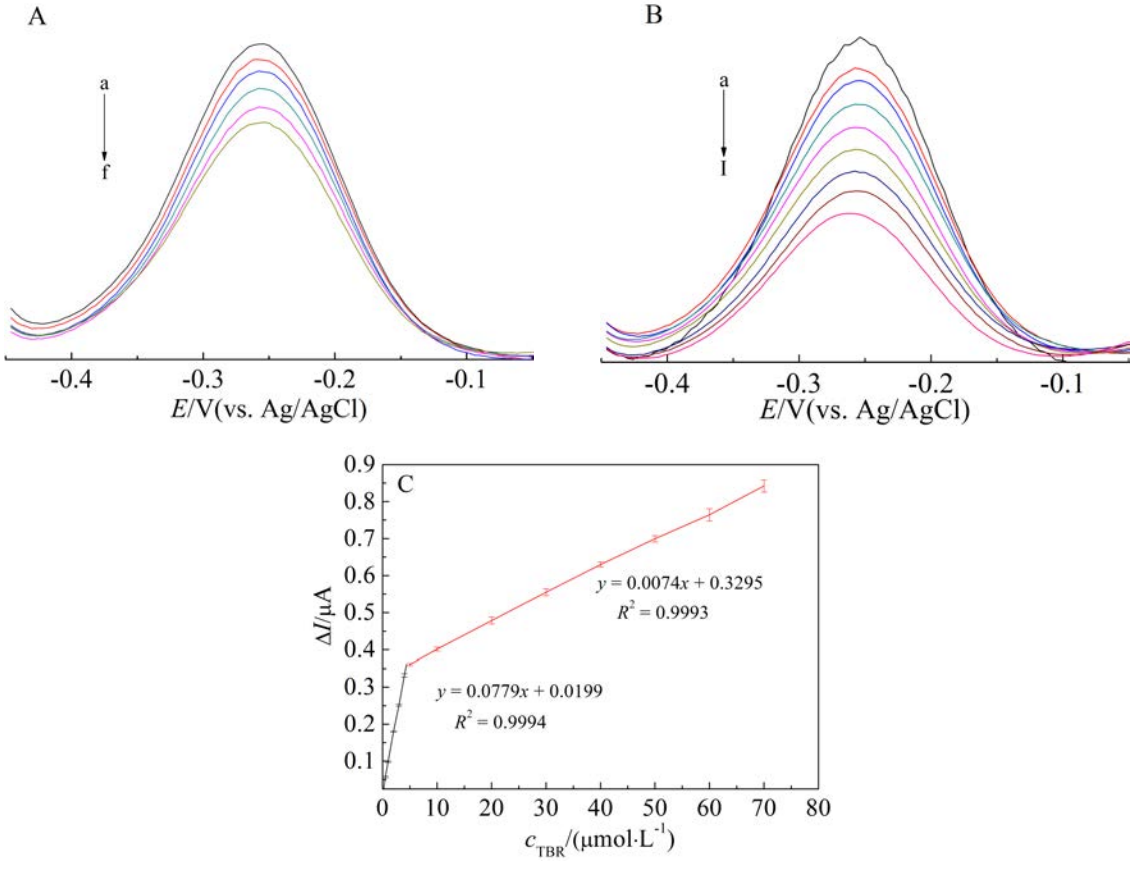

Fig. 4 DPVs of MB/Apt/AuNPs/PANI/TNTs/GC electrode after incubation for 40 min with different concentrations of tobramycin (from upper to down): 0.0, 0.5, 1.0, 2.0, 3.0 and 4.0 μmol·L^{-1} (A), 0, 5, 10, 20, 30, 40, 50, 60 and 70 μmol·L^{-1} (B). (C) is the plot of current response vs. tobramycin concentration.

Tab. 2 Performance of different aptamer-based tobramycin biosensors

Analytical method	Detection linear range/(μmol·L^{-1})	Detection limit / (μmol·L^{-1})	Ref.
Square wave voltammetry	0.2 ~ 42	-	Schoukroun-Barnes [10]
Impedimetric	3 ~ 72.1	-	González Fernández [11]
Surface plasmon resonance	0 ~ 80	0.3	Giulia Cappi [12]
Surface plasmon resonance	0.004 ~ 0.16	0.0038	Santos [13]
Differential pulse voltammetry	0.5 ~ 70	0.326	This work

teraction between TBR and aptamer hindered the electron transfer rate, and resulted in the signal decrease of MB. Maybe it is the synergetic effect of the two factors. By analyzing the peak currents of MB and the concentrations of tobramycin, a linear relationship was obtained. For the lower concentration range (0.5 ~ 4.0 μmol·L^{-1}), a linear equation was constructed as: ΔI(μA) = 0.0779 c(μmol·L^{-1}) + 0.0199, R^2 = 0.9994 (Fig. 4C), where ΔI means the difference of the current intensity in DPV of MB/Apt/AuNPs/PANI/TNTs/GC electrode and that of TBR/MB/Apt/AuNPs/PANI/TNTs/GC electrode, c means the concentration of tobramycin. For the higher concentration range (5 ~ 70 μmol·L^{-1}), the equation of ΔI(μA)= 0.0074 c(μmol·L^{-1}) + 0.3295, R^2 = 0.9993 (Fig. 4C) was built. A detection limit of 0.326 μmol·L^{-1} was achieved (based on S/N=3). The phenomenon of having two linear equations for different concentration ranges may be explained as follows: At lower concentrations, tobramycin interacted easily with the active sites of the aptamer. With an increase in the concentration of tobramycin, some active sites of the aptamer were occupied and so the sensitivity decreased, resulting in a smaller slope. Several studies had reported this phenomenon for other biosensors[28, 36-38]. Tab. 2 lists the performance of different aptasensors reported in other literatures. Compared with other studies, the aptasensor proposed here had excellent sensitivity and a relatively wide dynamic range for the detection of tobramycin.

The reproducibility of the proposed aptasensor is important for its application, and six MB/Apt/AuNPs/PANI/TNTs/GC electrodes were fabricated one by one and conducted for DPV analysis. A satisfactory relative standard deviation (RSD) of 5.5% was achieved. Additionally, the MB/Apt/AuNPs/PANI/TNTs/GC electrode was examined for six times. The RSD of the aptasensor responses was 3.9%. These results indicated that the electrochemical aptasensor described here had good reproducibility.

3 Conclusions

We have developed a simple electrochemical aptasensor for the detection of tobramycin with the AuNPs/PANI/TNTs nanocomposite as an electrode material. TEM results indicate that AuNPs with the average size of 4 nm dispersed uniformly on the surface of PANI/TNTs. Electrochemical characterization results showed that the AuNPs/PANI/TNTs nanocomposite resulted in the decreased R_{ct} value and facilitated the electron transfer. The results of DPV showed that the current of MB decreased linearly with the increase of the tobramycin concentration in the range of 0.5 to 70.0 μmol·L^{-1}; the estimated detection limit for tobramycin was 0.326 μmol·L^{-1}. The linear relationship between the current and the tobramycin concentration was well established. The proposed aptasensor provides a convenient, specific, and sensitive method for the detection of tobramycin, and can be potentially applied in bioanalysis and clinical diagnostics.

Acknowledgements

The project was supported financially by the National Natural Science Foundation of China (No. 21201043).

Supporting Information Available

The supporting information is available free of charge via the internet at http://electrochem.xmu.edu.cn.

References:

[1] Hammett-Stabler C A, Johns T. Laboratory guidelines for monitoring of antimicrobial drugs. National Academy of Clinical Biochemistry[J]. Clinical Chemistry, 1998, 44(5): 1129-1140.

[2] Zhang Y H(张玉红). Selection and sequence optimization of tobamycin specific single standard DNA aptamers and their applications[D]. JiangNan University, Jiang Su, 2017.

[3] Nederberg F, Zhang Y, Tan J P K, et al. Biodegradable nanostructures with selective lysis of microbial membranes[J]. Nature Chemistry, 2011, 3(5): 409-414.

[4] Stead D A. Current methodologies for the analysis of aminoglycosides[J]. Journal of Chromatography B: Biomedical Sciences and Applications, 2000, 747(1/2): 69-93.

[5] Shanson D C, Hince C J, Daniels J V. Rapid microbiologic assay of tobramycin[J]. Journal of Infectious Diseases, 1976, 134(supplement 1): S104-S109.

[6] Kang Y, Feng K J, Chen J W, et al. Electrochemical detection of thrombin by sandwich approach using antibody and aptamer[J]. Bioelectrochemistry, 2008, 73(1): 76-81.

[7] Wei N N, Xin X, Du J Y, et al. A novel hydrogen peroxide biosensor based on the immobilization of hemoglobin on three-dimensionally ordered macroporous (3DOM) gold-nanoparticle-doped titanium dioxide (GTD) film[J]. Biosensors & Bioelectronics, 2011, 26(8): 3602-3607.

[8] Ge F(戈芳), Cao R G(曹瑞国), Zhu B(朱斌), et al. DNA electrochemical biosensor for the detection of trace Hg^{2+} [J]. Acta Physico - Chimica Sinica(物理化学学报), 2010, 26(7): 1779-1783.

[9] Wang H J (王慧娟). Synthesis of ultrathin Co_3O_4 nanoflakes film material for electrochemical sensing[J]. Journal of Electrochemistry(电化学), 2016, 22(6): 631-635.

[10] Schoukroun-Barnes L R, Wagan S, White R J. Enhancing the analytical performance of electrochemical RNA aptamer-based sensors for sensitive detection of aminoglycoside antibiotics[J]. Analytical Chemistry, 2014, 86(10): 1131-1137.

[11] Gonzalez-Fernandez E, de-los-Santos-Alvarez N, Lobo-Castanon M J, et al. Impedimetric aptasensor for tobramycin detection in human serum[J]. Biosensors & Bioelectronics, 2011, 26(5): 2354-2360.

[12] Cappi G, Spiga F M, Moncada Y, et al. Label-free detection of tobramycin in serum by transmission-localized surface plasmon resonance[J]. Analytical Chemistry, 2015, 87(10): 5278-5285.

[13] Santos H S, de França G M, Romani E C, et al. Selective determination of tobramycin in the presence of streptomycin through the visible light effect on surface plasmon resonance of gold nanoparticles[J]. Microchemical Journal, 2014, 116: 206-215.

[14] Wang M H, Hu B, Yang C, et al. Electrochemical biosensing based on protein-directed carbon nanospheres embedded with SnO_x and TiO_2 nanocrystals for sensitive detection of tobramycin[J]. Biosensors and Bioelectronics, 2018, 99: 176-185.

[15] Wang Y, Rando R R. Specific binding of aminoglycoside antibiotics to RNA[J]. Chemistry & Biology, 1995, 2(5): 281-290.

[16] Jiang L, Suri A K, Fiala R, et al. Saccharide-RNA recognition in an aminoglycoside antibiotic-RNA aptamer complex[J]. Chemistry & Biology, 1997, 4(1): 35-50.

[17] Tuite E, Norden B. Sequence-specific interactions of methylene blue with polynucleotides and DNA: A spectroscopic study[J]. Journal of the American Chemical Society, 1994, 116(17): 7548-7556.

[18] Kerman K, Ozkan D, Kara P, et al. Voltammetric determination of DNA hybridization using methylene blue and self-assembled alkanethiol monolayer on gold electrodes [J]. Analytica Chimica Acta, 2002, 462(1): 39-47.

[19] Kara P, Kerman K, Ozkan D, et al. Electrochemical genosensor for the detection of interaction between methylene blue and DNA[J]. Electrochemistry Communications, 2002, 4(9): 705-709.

[20] Li X Y, Lu X J, Kan X W. 3D electrochemical sensor based on poly(hydroquinone)/gold nanoparticles/nickel foam for dopamine sensitive detection[J]. Journal of Electroanalytical Chemistry, 2017, 799: 451-458.

[21] Li P(李培), Zhan D P(詹东平), Shao Y H(邵元华). Room temperature ionic liquid templated meso-macroporous material by self-assembled giant gold nanoparticles and its enhancement on room temperature ionic liquid templated meso-macroporous material by self-assembled giant gold nanoparticles and its enhance[J]. Journal of Electrochemistry(电化学) 2014, 20(4): 323-332.

[22] Huang Z J(黄郑隽), Peng H P(彭花萍), Zha D J(查代君), et al. Electrocatalytic activities of Mb/AuNPs/MWCNTs/GC electrode for hydrogen peroxide reduction[J]. Journal of Electrochemistry(电化学), 2012, 18(4): 377-382.

[23] Pavlov V, Xiao Y, Shlyahovsky B, et al. Aptamer-func-

tionalized Au nanoparticles for the amplified optical detection of thrombin[J]. Journal of the American Chemical Society, 2004, 126(38): 11768-11769.

[24] Chen J, Kang Y, Li C, et al. A Pt/TiO_2 nanotube array electrode for glucose detection and its photoelectrocatalysis self-cleaning ability[J]. Journal of The Electrochemical Society, 2016, 164(2): B66-B73.

[25] Huo X H, Liu P P, Zhu J, et al. Electrochemical immunosensor constructed using TiO_2 nanotubes as immobilization scaffold and tracing tag[J]. Biosensors and Bioelectronics, 2016, 85: 698-706.

[26] Liu N, Chen X Y, Zhang J L, et al. A review on TiO_2-based nanotubes synthesized via hydrothermal method: Formation mechanism, structure modification, and photocatalytic applications[J]. Catalysis Today, 2014, 225(225): 34-51.

[27] Zhang Z, Luo L Q, Zhu L M , et al. Aptamer-linked biosensor for thrombin based on AuNPs/thionine-graphene nanocomposite[J]. Analyst, 2013, 138(18): 5365-5370.

[28] Khezrian S, Salimi A, Teymourian H, et al. Label-free electrochemical IgE aptasensor based on covalent attachment of aptamer onto multiwalled carbon nanotubes/ionic liquid/chitosan nanocomposite modified electrode [J]. Biosensors and Bioelectronics, 2013, 4: 218-225.

[29] Liu X Q, Zhang J M, Liu S H, et al. Gold nanoparticle encapsulated-tubular TiO_2 nanocluster as a scaffold for development of thiolated enzyme biosensors[J]. Analytical Chemistry, 2013, 85(9): 4350-4356.

[30] Liu X Q, Yan R, Zhang J M, et al. Evaluation of a carbon nanotube-titanate nanotube nanocomposite as an electrochemical biosensor scaffold[J]. Biosensors & Bioelectronics, 2015, 66: 208-215.

[31] Yan M Q, Shen Y, Zhang G Y, et al. Multifunctional nanotube-like Fe_3O_4/PANI/CDs/Ag hybrids: An efficient SERS substrate and nanocatalyst[J]. Materials Science and Engineering: C, 2016, 58: 568-575.

[32] Zhou X, Shi T J, Wu J, et al. (0 0 1) Facet-exposed anatase-phase TiO_2 nanotube hybrid reduced graphene oxide composite: Synthesis, characterization and application in photocatalytic degradation[J]. Applied Surface Science, 2013, 287(2): 359-368.

[33] Sim L C, Leong K H, Saravanan P, et al. Rapid thermal reduced graphene oxide/Pt-TiO_2 nanotube arrays for enhanced visible-light-driven photocatalytic reduction of CO_2[J]. Applied Surface Science, 2015, 358, Part A: 122-129.

[34] Yang K, Huang K, He Z J, et al. Promoted effect of PANI as electron transfer promoter on CO oxidation over Au/TiO_2[J]. Applied Catalysis B: Environmental, 2014, 158(3): 250-257.

[35] Li X Z, Liu W, Ni J R. Short-cut synthesis of tri-titanate nanotubes using nano-anatase: Mechanism and application as an excellent adsorbent[J]. Microporous and Mesoporous Materials, 2015, 213: 40-47.

[36] Yang H, Ji J, Liu Y, et al. An aptamer-based biosensor for sensitive thrombin detection[J]. Electrochemistry Communications, 2009, 11(1): 38-40.

[37] Dong X X, Li M Y, Feng N N, et al. A nanoporous MgO based nonenzymatic electrochemical sensor for rapid screening of hydrogen peroxide in milk[J]. RSC Advances, 2015, 5(105): 86485-86489.

[38] Ding C, Ge Y, Lin J M. Aptamer based electrochemical assay for the determination of thrombin by using the amplification of the nanoparticles[J]. Biosensors and Bioelectronics, 2010, 25(6): 1290-1294.

基于 AuNPs/PANI/TNTs 纳米复合材料的电化学检测妥布霉素的适配体传感器

农永玲[1],乔妮娜[1],梁 营[1,2*]

(1. 广东药科大学医药化工学院,广东 广州 510006; 2. 广东省化妆品工程技术研究中心, 广东 广州 510006)

摘要:本文提出了一种新型的检测妥布霉素的电化学适配体传感器,以差分脉冲伏安法(DPV)作为检测技术,亚甲基蓝作为电化学响应信号. 构建了以纳米复合材料金纳米粒子/聚苯胺/二氧化钛纳米管(AuNPs/PANI/TNTs)修饰玻碳电极的电极支架. 通过透射电子显微镜和 X-射线光电子能谱对纳米复合材料进行详细的表征. 循环伏安图和电化学阻抗谱显示 AuNPs/PANI/TNTs 可以很好地增加电极的界面传导性能. DPV 结果显示电流密度的响应和妥布霉素浓度之间存在一个很好的线性关系,并且得到一个宽广的检测范围为 0.5 μmol·L^{-1} 到 70 μmol·L^{-1}. 本文提出的适配体基的传感器有很好的重复性和稳定性, 作为一个潜在的手段可以应用在生物分析和医疗诊断中.

关键词:适配体;妥布霉素;电化学分析;金纳米粒子